Development of a Plasma Solver for Surge Protective Devices using Spark Gap Technology

Sander C.[1], Rüther J.[2], Kurrat M.[2]

[1]PHOENIX CONTACT GmbH & Co. KG, Flachsmarktstraße 8, D-32825 Blomberg, Germany, christian.sander1@phoenixcontact.com

[2]Technische Universität Braunschweig, Institute for High Voltage Technology and Electrical Power Systems, Schleinitzstraße 23, 38106 Braunschweig, Germany, m.kurrat@tu-braunschweig.de

In this article we present the development of a single-fluid plasma model using the open-source CFD-based modelling framework OpenFOAM for the simulation of surge protective devices. The model uses a pressure based flow solver and supports the use of common radiation models such as the P1 model. Empirical models for electrode sheaths can be used and coupling the simulation to external circuits is possible. Some initial results are presented and compared with high-speed camera recordings.

Keywords: spark gap, simulation, plasma, arc, lightning, surge protective device

1 INTRODUCTION

The efficient development of surge protective devices (SPD) requires the knowledge of the underlying physics of thermal plasmas. SPDs can fail due to high mechanical stress, so the understanding of flow and pressure build-up is of vital importance.

Plasma simulations are very common in the development of circuit breakers [1] and welding applications [2]. The physics in these fields are similar to SPDs, but they usually have lower currents and thus lower power densities, temperatures and pressures. Small geometries and high impulse currents (up to 50 kA) in SPDs lead to a larger stress being imposed. However, the number of operating cycles is much lower compared to circuit breakers and the common duration of an electrical surge is less than 1 ms. This leads to a much more dynamic behaviour in SPDs.

Here we present the development of a plasma model used for SPDs. We give an overview over the involved physics and present some initial results on a model spark gap, using a high speed camera to examine the behaviour of the plasma flow.

2 PHYSICS OF SURGE PROTECTIVE DEVICES

The physics of plasma discharges in spark gaps allow making some basic assumptions:

- The plasma is in local thermodynamic equilibrium
- The plasma is quasi-neutral
- Transient electromagnetic terms in the Maxwell equations may be neglected on µs-timescales
- Magnetic advection may be neglected because of low magnetic Reynolds numbers

This makes it possible to treat the plasma as a single fluid. Balance equations can then be used for mass, momentum and energy.

$$\frac{\partial \rho}{\partial t} + \nabla \cdot \left(\rho \cdot \vec{U}\right) = S_m \tag{1}$$

$$\frac{\partial \rho \vec{U}}{\partial t} + \nabla \cdot \left(\rho \vec{U} \vec{U}\right) = -\nabla p + \nabla \cdot \tau + \vec{j} \times \vec{B} + \vec{S_i} \tag{2}$$

$$\frac{\partial \rho (e+k)}{\partial t} + \nabla \cdot \left((\rho(e+k)+p)\vec{U} - \alpha \nabla e\right) = \tau \vec{U} + \vec{j} \cdot \vec{E} + S_{Rad} + S_e \tag{3}$$

Above we denote with ρ the density, $\vec{U}$ the velocity, p the pressure, τ the impulse stress tensor, e the internal energy, k the kinetic energy and α the thermal diffusivity.

These equations have the form of compressible Navier-Stokes equations with additional source terms. Most important are the Lorentz force $\vec{j} \times \vec{B}$, which leads to thinner arc diameters, the joule heating term $\vec{j} \cdot \vec{E}$ and the radiative energy term S_{Rad}, which is responsible for the majority of heat transfer in the plasma. Additional source terms (S_m, $\vec{S_i}$ and S_e) may be present depending on the used submodels. These will be explained later in

this section.

The electromagnetical source terms are calculated from the Maxwell equations in the static limit. This means that all time dependent terms are neglected because their magnitude is low in the frequency range of current impulses commonly found in surge protection applications (less than 1 MHz).

$$\nabla \cdot (\sigma \nabla \Phi) = 0 \tag{4}$$

$$\Delta \vec{A} = \mu_0 \mu_R \vec{j} \tag{5}$$

Here we denote with σ the electrical conductivity, Φ the electric potential, $\vec{A}$ the magnetic vector potential, μ_0 the vacuum permeability, μ_R the relative permeability and $\vec{j}$ the current density. Using the relations $\vec{j} = \sigma \vec{E} = -\sigma \nabla \Phi$ and $\vec{B} = \nabla \times \vec{A}$, the coupling with equations (2) and (3) is complete. If the permeability is locally different because of magnetic materials other formulations need to be used [3].

By treating the plasma as a single fluid it becomes necessary to use integrated material properties that are valid for the local state of the plasma (the composition, temperature and pressure). These properties are the equation of state ρ(p, T), the enthalpy h(p, T), the thermal diffusivity α(p, T), the viscosity ν(p, T) and the electrical conductivity σ(p, T). The enthalpy function can be inverted to determine the temperature. The effect of different plasma compositions on the material properties can be considered in the form of mixing laws [4].

The radiative transfer equation [5] has to be solved for the radiative energy source term:

$$\hat{s} \cdot \nabla I_\nu(\vec{r}, \hat{s}) = \kappa_\nu (B_\nu - I_\nu) \tag{6}$$

In this equation, $I_\nu(\vec{r}, \hat{s})$ is the spectral radiative intensity at the point $\vec{r}$ and in the direction $\hat{s}$. κ_ν is the spectral absorption coefficient and B_ν is the Planck intensity.

Unfortunately, the numerical effort to solve this equation is too high to be performed in a three-dimensional simulation so an approximation is needed. We use the common P1 method, which is appropriate for optically thick mediums:

$$I_\nu(\vec{r}, \hat{s}) \approx \frac{1}{4\pi}(G_\nu(\vec{r}) + 3\hat{s} \cdot \overrightarrow{F_\nu}(\vec{r})) \tag{7}$$

$$\overrightarrow{F_\nu}(\vec{r}) = -\frac{1}{3\kappa_\nu} \nabla G(\vec{r}) \tag{8}$$

$$\nabla \cdot \left(\frac{1}{3\kappa_\nu} \nabla G_\nu\right) = \kappa_\nu (G_\nu - 4\pi B_\nu) \tag{9}$$

$$S_{Rad} = \int \nabla \cdot F_\nu d\nu \tag{10}$$

With $G_\nu(\vec{r})$ we denote the incident radiation and with $\overrightarrow{F_\nu}(\vec{r})$ the radiative heat flux.

In the plasma encountered in spark gaps, the P1 approximation is often valid because the high pressures encountered in the small housings lead to a high absorption coefficient, and so the plasma can be considered as optically thick in most cases. This, combined with the good numerical performance makes this the method of choice.

The P1 method requires a spectral discretization. Optical absorption spectra are very irregular so the process of averaging is a delicate task that can lead to large errors [6]. The simplest approach is to divide the absorption spectrum in multiple bands, for which the P1 equation is solved separately. This can lead to acceptable numerical errors.

The radiative (and to some extent thermal) energy transfer to the walls causes an ablation process. SPDs often use polyoxymethylene (POM) as wall material. Material ablation leads to constricted arcs with a smaller cross section and hence a higher resistance. The additional mass cools the plasma and leads to a pressure increase which adds additional mechanical stress on the housing. The material ablation rate is estimated by the total incoming heat flux:

$$\dot{m} = \frac{q_{Rad} + q_{H,in} - q_{H,out}}{\Delta h_{POM}} A \tag{11}$$

Here q_{Rad} is the incoming radiative heat flux density normal to the wall and $q_{H,in}$ is the heat flux due to heat conduction towards the wall. $q_{H,out}$ is the heat flux into the solid which can be calculated with a heat conduction equation and the assumption that the surface temperature does not exceed the evaporation temperature. Δh_{POM} is the specific evaporation

enthalpy of POM and A is the surface area of an outermost cell at the wall. It is possible to neglect $q_{H,out}$ and skip the heat conduction equation to save computational time. This leads to an overestimation of ablated material. The source term for equation (1), $S_{m,POM} = \frac{\dot{m}}{V_{Cell}}$, is added in the outer cell layer at the polymer walls. The impulse source term is given as $\overrightarrow{S_i} = \frac{d\vec{p}}{dt} = \dot{m}\vec{U} = \frac{\dot{m}^2}{\rho A}\hat{n}$. Here $\vec{p}$ is the momentum and $\hat{n}$ is the unit vector normal to the wall, pointing into the plasma volume. Finally, the energy source term due to ablation is derived as $S_e = S_m \Delta h_{POM}$.

At the contact between the plasma and the electrode the assumptions that allow the treatment of the plasma as a single fluid are no longer valid. Instead a plasma sheath layer forms with a thickness in the range of a Debye length. The plasma is no longer in local thermodynamic equilibrium, as the emitted particles have a different energy distribution compared to the bulk plasma and the different speeds of electrons and ions leads to a violation of the quasi-neutrality. Because of the small size of this layer a full scale physical model is not feasible and so the empirical model proposed by Lindmayer [7] is used. This model is based on a modified conductivity in the first cell layer that accounts for the voltage drop across the plasma sheath layer.

3 DESCRIPTION OF THE SOLVER

This plasma model is based on the open source CFD modelling framework OpenFOAM using the finite volume method. As a basis for the plasma model we have chosen the pressure-based sonicFoam solver, which performs best at subsonic speeds, but also provides acceptable results in supersonic cases [8]. The solver is extended according to the last chapter. We apply an adaptive time stepping method based on the Courant number. The plasma model can be coupled to an external electrical circuit using a script that solves the equations of the external circuit.

The material properties for air plasmas from D'angola [9] are used because they are calculated over a wide range of pressures and temperatures. The absorption spectra for air were calculated using the line by line radiation program SPARTAN [10]. In this report the Rosseland average with 6 bands using the ranges from Rümpler [11] was used. Material properties for POM and Cu were not available to us at the time of this publication.

4 INITIAL RESULTS AND DISCUSSION

For an initial evaluation we have performed simulations on a simple geometry for which high speed camera images were recorded. The geometry consists of two rail electrodes at a distance of 5 mm and a width of 1 mm (left and right sides on the images in Fig. 1). The rectangular plasma volume between the electrodes is open at the top side. The front and back sides are covered with POM and with polymethylmethacrylat (PMMA) that allows to record images of the plasma. The plasma is ignited using a third electrode near one of the main electrodes at the bottom. Further information regarding the experimental setup and the camera are provided by Schottel [12].

A hexahedral mesh with approximately 120 000 cells is used with cell sizes of 16-167 µm. The simulation is started with a uniform temperature and pressure distribution after the ignition estimated from the camera images and zero velocity. A measured current impulse is impressed.

The simulated voltage curve in Fig. 1 only gives a qualitative agreement. There are multiple reasons for this: The conditions of the plasma after the ignition are only estimated, especially the velocity field is expected to be vastly different in the simulation compared to reality. Including the ignition process in the simulation is expected to help but wasn't implemented yet. The used voltage curves for the sheath model are inspired from previous works on circuit breakers with much lower currents. However, our experimental results indicate that the sheath voltages might be higher. The measured ablation mass (250 µg ± 20%) is five times larger than the simulated value (51 µg). Higher ablation is known to increase the voltage, so this contributes to the lower simulated voltage. Finally, treating the plasma as air is likely to lead to deviations as

well. However, concerning the simplifications, the agreement is satisfying.

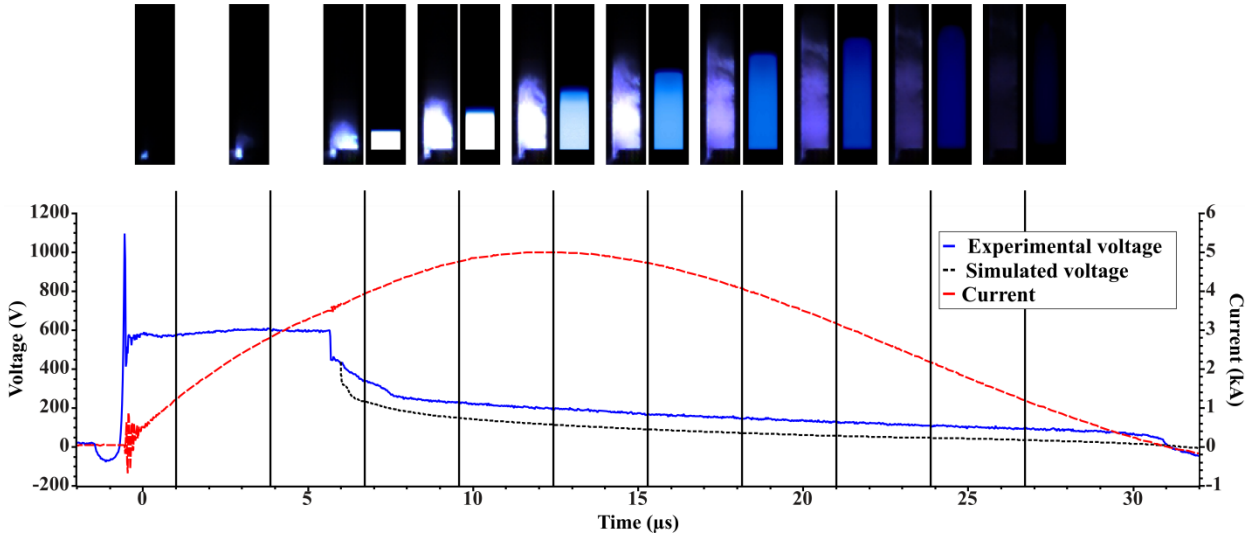

Fig. 1: Top: Camera images (left) and simulated radiative heat flux (right) of the spark gap; Bottom: Experimental and simulated voltage curves for a 5 kA impulse

For better visibility at the end of the impulse, the simulated radiative heat flux is displayed on a logarithmic scale. The simulation shows a similar expansion speed compared to the camera images, but the flow is steadier, which is partially caused by the initial conditions and the neglect of turbulences in the model. The simulation shows a continuous electrode sheath without single foot points during the whole impulse. It doesn't decompose into single foot points near the current zero like other camera images demonstrate. It is not likely that the current model will be able to capture this properly, so an improved model should be developed in the future.

5 CONCLUSION

In its current state the model can already produce qualitative results that can be used in the development process. Further work will be needed on electrode sheaths, material properties and the ignition process to get more accurate results. The progress on these topics will be reported in a future article.

REFERENCES

[1] Freton P, Gonzalez J J, Open Plasma Physics Journal 2 (2009), 105-119.
[2] Lu F et al., Comp Mat Sci 35 (2006), 458-465.
[3] Rondot L et al., IEEE Trans Magn 45 (2009) 1262-1265.
[4] Gleizes A et al., Plasma Sources Sci Technol 19 (2010) 055013.
[5] Modest M F, Radiative heat transfer, Academic press (2013).
[6] Nordborg H, Iordanidis A A, J. Phys. D: Appl. Phys. 41 (2008) 135205.
[7] Lindmayer M et al., IEEE Trans. Compon. Packag. Technol. 29 (2006) 310-317.
[8] Gutiérrez Marcantoni L F et al., Mecánica Computacional 31 (2012) 2939-2959
[9] D'angola A et al., Eur. Phys. J. D 46 (2008) 129-150.
[10] da Silva M L, J. Quant. Spectrosc. Radiat. Transfer 108 (2007) 106-125.
[11] Rümpler C et al., In: 57th Conference on Electrical Contacts, Holm, IEEE, 2011, 1-8.
[12] Schottel B et al., In: International Conference on Lightning Protection, Shanghai, 2014, 1400-1404.